JOURNAL OF AIRCRAFT
Vol. 47, No. 2, March–April 2010

Modeling, Simulation, and Flight Tests for a T-38 Talon with Wing Fences

Michael D. Williams,* Mark F. Reeder,† Raymond C. Maple,‡ and Daniel A. Solfelt§
Air Force Institute of Technology, Wright–Patterson Air Force Base, Ohio 45433-7542

DOI: 10.2514/1.46122

A computational study, a wind-tunnel analysis, and a flight test on the T-38 Talon demonstrated that approach-to-stall characteristics may be improved by the addition of a wing fence. Fences were placed at the location of a preexisting seam, at ±0.825 semispan, and were compared with the T-38 without fences. Reynolds-averaged Navier–Stokes simulations were conducted using the computational fluid dynamics air vehicles unstructured solver to examine the flow around the T-38 at typical full-flap landing conditions ($Re = 4.66 \times 10^6$ per unit length). Solutions were computed over a range of angles of attack from 2 to 15 deg. The fence was found to increase $C_{L\max}$ by 7% and delay the attainment of $C_{L\max}$ from a 12 to a 13 deg angle of attack. This effect was achieved through the formation of a discrete streamwise vortex outboard of the fence, which prevented flow separation in the tip region, which (in turn) delayed flow separation over the remainder of the wing, resulting in the higher computed lift. Wind-tunnel results, by and large, were based on aircraft instrumentation and flow visualization for Mach numbers up to 0.65 ($Re_{\text{mac}} \sim 10^7$). The flight-test data showed an increase in C_L of approximately 2% in the angle-of-attack range of 12–14.5 deg when the wing fence was in place. Onboard accelerometer data suggest the fence reduced the roll-off tendency and the wing-rock amplitude during approaches to stall. Flow visualization on the aircraft wing in both the wind-tunnel study and the flight test suggested that the fence reduced spanwise and separated flow outboard the fence, which agreed with the computational fluid dynamics results.

Nomenclature

C_L	=	lift coefficient
$C_{L\max}$	=	maximum lift coefficient
Re	=	Reynolds number
Re_{mac}	=	Reynolds number based on mean aerodynamic chord length
X	=	streamwise direction
Y	=	lateral direction
Z	=	vertical direction

I. Introduction

NORTHROP Grumman built the T-38 Talon, a twin-engine supersonic fighter-type jet, and delivered more than 1100 aircraft. The T-38 first flew in March 1959 and was fielded in 1961. The U. S. Air Force (USAF) and NASA use the aircraft extensively in a variety of roles. The aircraft is undergoing several programs designed to: increase its structural service life to 2020, improve training, increase thrust, and improve engine reliability and maintainability [1]. Therefore, it is a logical time to investigate modifications to improve the aircraft's high angle-of-attack (AOA) performance and approach-to-stall characteristics. Ultimately, such improvements can improve training, safety, and life-cycle costs. One such modification, the addition of a wing fence, was proposed by Roger Tanner, a test pilot in the 416th Flight Test Squadron at Edwards Air Force Base (AFB) and the USAF Test Pilot School (TPS).

Wing fences have been used to improve approach-to-stall characteristics on a myriad of aircraft, including the combat-capable F-5F, an aircraft that is very similar to the T-38. Other examples of fence use include the MiG-15, the F-86, the Fiat G91, and the BAE Systems Hawk and Harrier. Fences have been used for more than 70 years in aviation, and the individual credited with the invention of the wing fence is Wolfgang Liebe [2]. He received a German patent in 1938 for his work on the Messerschmitt Bf 109B. The stall characteristics of the Bf 109B were peculiar, but they were countered by the installation of a fence that prevented cross-span flow. The wing fence has been a widely used device, especially for swept-wing aircraft, and was a good candidate here. Wind-tunnel visualization and theoretical studies suggest that a wing fences produces a vortex outboard of the fence that rotates in the opposite direction to the wing-tip vortex [3,4].

Unlike wings composed of more common airfoil sections, the T-38 wing does not encounter a hard break in the lift curve. Rather, the stall condition is immediately preceded by heavy low-speed buffet and moderate wing rock, and the stall is characterized by airframe buffet and a high sink rate, rather than by a clean nose-down pitch motion [5]. This behavior sets the T-38 wing apart from most aircraft. The T-38's airfoil is a NACA 65A004.8 with a 1% chord-contrast leading-edge droop. It is trapezoidal in shape, with a planform area of 170 ft^2, a wing span of 25.25 ft., and an aspect ratio of just 3.75. With a very thin wing, it has a maximum thickness ratio of just 4.8%. The leading-edge and quarter-chord wing sweeps are 32 and 24 deg, respectively. Dihedral and incidence angles are both 0 deg. These characteristics significantly contribute to the aircraft's high-AOA behavior [5].

Significant factors when considering the test effort are aircraft modification time and cost. In this regard, a wing fence is attractive, because the T-38 has a row of fasteners that span the chord of the airfoil at 0.825 semispan. This row of fasteners provides a relatively easy location to attach a fence, with little or no structural changes to the wing. Other flow control devices, such as vortex generator vanes or other fence positions, would have required much more extensive modifications to the clean aircraft.

An important question to be answered was whether or not wing fences placed at a 0.825 semispan on each wing improved high-AOA

Received 24 June 2009; revision received 20 August 2009; accepted for publication 31 August 2009.

*Major, U.S. Air Force, Department of Aeronautics and Astronautics, Building 640; currently Test Pilot, 419 Flight Test Center, Edwards Air Force Base, California. Member AIAA.

†Associate Professor, Department of Aeronautics and Astronautics, Building 640. Member AIAA.

‡Assistant Professor, Department of Aeronautics and Astronautics, Building 640; currently Advanced Design Team Engineer, Hawker Beechcraft Corporation. Senior Member AIAA.

§Graduate Student, Department of Aeronautics and Astronautics, Building 640; also Ensign, U.S. Navy.

performance and approach-to-stall characteristics for the T-38, especially given its low aspect ratio and the significant wing taper. An early study of wing fences mounted on a wing with less taper suggested that a fence positioned as far outboard as 0.76 semispan "would increase the lift coefficient for angles greater than about 10 deg by delaying the lift break to higher angles of attack" [6]. In fact, the effect of the fence on the lift curve was shown to become more substantial as the fence semispan position was increased from 0.65 to 0.76, so that there was reason to believe that the wing fence at the 0.825 semispan location would be effective in delaying the lift break. However, the differences in the wing described in [6] were profoundly different from that of the T-38, and a full investigation was required to determine the true effect of a fence. Therefore, tests comprising CFD studies, wind-tunnel runs, and flight tests were undertaken.

II. Methodology

A. Computational Fluid Dynamics Study

The study was conducted using the air vehicles unstructured flow solver (AVUS), formerly known as Cobalt-60 [7]. Solutions were generated with and without a fence, and the resulting flowfields and lift curves were compared. The study focused on AOA only, and no attempt was made to examine the effects of sideslip on fence performance. Simulations modeled T-38 landing air conditions, for which it was assumed high-AOA conditions would be encountered. Freestream conditions applied were Mach = 0.2, density= 101, 325 Pa, and temperature = 288 K, corresponding to a $Re = 4.66 \times 10^6$ per unit length and approximating minimum T-38 touchdown speeds. An isometric view of the solid model used in the simulation is given in Fig. 1. The engine inlet and exhaust were modeled as sink and source boundary conditions using mass flow and pressure specifications. Engine idle conditions were simulated, with an inlet mass flow of 6.69 kg/s, exhaust conditions of 104,109 Pa total pressure, and 791 K total temperature. Engine inlet and outlet flows were assumed to be uniform and without swirl. Full-flap conditions were approximated by rotating the flap portion of the trailing edge down 45 deg to create a simple flap. The wing fence was added at 0.825 semispan. The fence wrapped around the leading edge of the wing and extended approximately 84.6% of the local chord length along the upper surface. The fence height was 2.5 in. Its base width was 0.5 in. and tapered to sharp edges. To reduce the size of the computational problem, the T-38 was modeled as a half aircraft with a symmetry plane cutting down its centerline. In addition, the CAD data for the T-38 did not include the tail section, and so the aircraft was modeled without empennage. As a result, direct comparison of results with existing T-38 data and investigation of the fence's impact on stability were not practical.

Unstructured computational grids were generated in a two-stage process using the programs GRIDGEN (grid generator) and SolidMesh/AFLR3 (advancing-front/local-reconnection three-dimensional unstructured grid generator) from the Engineering Research Center and SimCenter at Mississippi State University [8,9]. CAD geometry clean up and surface mesh generation were performed with GRIDGEN. Surface meshes over the fuselage and the inner wing were similar for the clean (no-fence) and fence models. Including the fence geometry required refinement of the surface mesh in the vicinity of the fence. In addition, the mesh outboard of the fence was refined to better resolve the flow in that region. Final surface meshes contained approximately 206,000 triangles with the clean wing and 278,000 triangles with the fence. Surface meshes were exported to SolidMesh for volume grid generation. SolidMesh/AFLR3 was used to automatically generate a boundary-layer mesh of anisotropic prisms, transitioning to an isotropic tetrahedral mesh away from the aircraft body. A target y^+ of 1.5 for the first node off the wall, at $Re = 10.0 \times 10^6$, was used. The resulting average y^+ at the wall, reported by AVUS, was less than 1.5 in all cases. The grid was extended five aircraft lengths above, below, and in front of the fuselage, six lengths behind the fuselage, and five lengths out from the wing tip. The final grids used for the results presented in this paper contained 5.1 and 6.6 million cells for the clean and fenced aircraft, respectively. To ensure the grids described previously were sufficiently refined, a 12.5 million-cell fence grid was constructed. Lift coefficient data from solutions on this fine grid differed from the 6.6 million-cell grid by less than 1% [10]. All flow solutions were computed with AVUS, using steady-state second-order spatial accuracy settings. Though not ideal for the massively separated flow expected, the Spalart–Almaras turbulence model was selected for its robustness. An unsteady detached-eddy simulation (DES) model was considered but rejected, due to the added grid generation complexity, the increased computational time, and the limited perceived benefit. Prior studies have shown that Reynolds-averaged Navier–Stokes solutions are capable of capturing the relevant flow physics to examine changes in mean lift and drag in high-AOA simulations, producing results similar to DES solutions [11,12]. Solution convergence was determined by monitoring the integrated forces on all wall boundaries, as reported by AVUS. These forces were observed to converge over many iterations in an oscillatory manner, with a period of approximately 200–300 iterations. Solutions were converged until the variation in the integrated normal force (Z component) varied by less than 1% over the final 400 iterations. Most solutions achieved a normal force variation of approximately 0.2%. Variations in axial (X component) force were typically higher, in the range of 1–2%. Density residuals were also checked and typically converged by approximately three orders of magnitude.

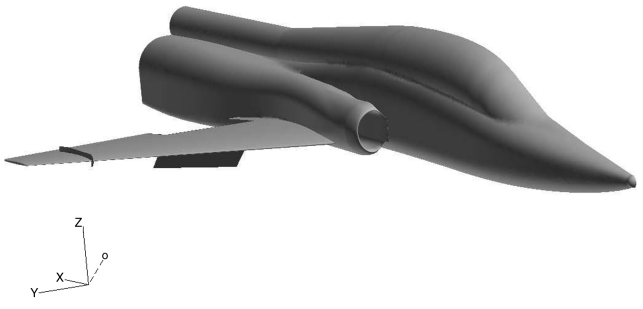

Fig. 1 CFD-modeled T-38 geometry with fence.

B. Wind-Tunnel Experiment Setup

Four analyzed configurations are pertinent here. Those are the model with and without wing fences and a tufted-wing model with and without fences. An analysis using trip tape was accomplished, but the results were insignificant [13]. The wind-tunnel model, modified from the geometry used in the CFD study, was produced on the Air Force Institute of Technology's (AFIT's) Objet Eden^{TM} 500 V rapid-prototype machine with VeroBlue material. It was 22.05 in. long, had a wing span of 14.43 in., and weighed 3.3 lbs. The size was chosen, based upon rapid-prototyping equipment, structural and aeroelastic considerations, and wind-tunnel balance constraints. It was a 1:21 scale model that did not include the tail. The omitted length was the last 4.45 in. of the model, which was equivalent to the last 7.79 ft of the aircraft. A photograph of the complete model and a close-up of the test fence are shown in Fig. 2. This fence extended 84.6% of the local chord along the wing's upper surface, wrapped the leading edge, and extended from the leading edge to 15% of the local chord length on the lower wing surface.

The method for changing between the baseline model and the model with wing fences was also incorporated into the drawings. One fuselage with interchangeable wings was used. The wings were one solid piece, tip to tip, as seen in Fig. 3. This was accomplished by slicing a rectangular piece out of the bottom side of the fuselage, corresponding to the leading and trailing edges of the wing. To aid in consistent alignment, a block was extruded from the fuselage and included as a part of the wing. Because of the small size of the scaled fences (0.119 in. tall and 0.03 in. thick), the fences were drawn as part of the wing and built by the three-dimensional printer as one piece.

Tufts were the technique of choice for flow visualization and were applied to the clean and fence configurations. Scotch® tape and small

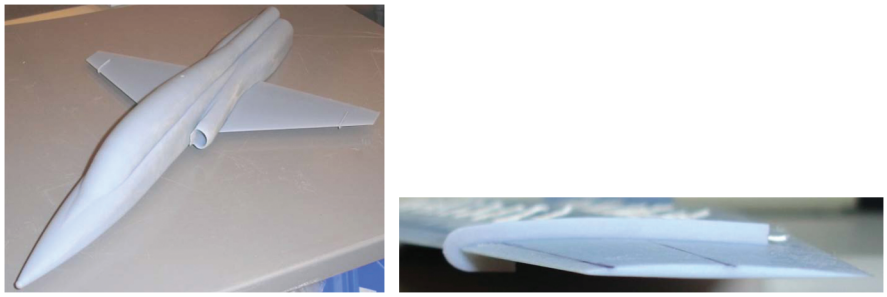

Fig. 2 Photograph of T-38 wind-tunnel model and the test fence.

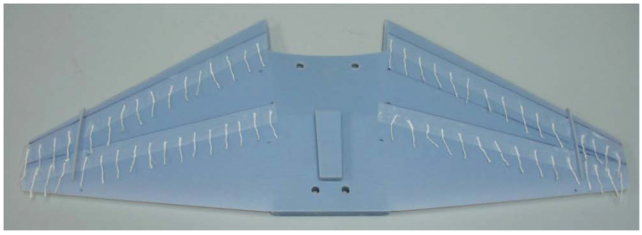

Fig. 3 Wind-tunnel model wing tufting.

filaments of yarn were used at a length of 0.5 in. Two rows were positioned on the upper surface. The first row covered (start of tuft to end of tuft) 19 to 29% of the chord at the root and 49 to 88% of the chord at the tip. The second row covered 58 to 68% of the chord at the root and 88 to 127% of the chord at the tip. Pictures of tufting can be seen in Fig. 3.

The tests completed in this study used the AFIT low-speed open-circuit wind tunnel. Models were mounted to an internal balance that was attached to a movable sting in the test section of the tunnel. The sting was adjusted by a movable control table and a pitch control device. Force and moment measurements were taken by the balance, once the wind tunnel reached the desired velocity. AOA sweeps were accomplished by pitching the balance and model via the stepper motor, accessed using National Instruments™ LabVIEW. This motor and linkage were located underneath the tunnel. Data were acquired through the use of a computerized data acquisition system. The acquisition recorded the following values: AOA, sideslip, tunnel speed, unresolved normal force, unresolved axial force, side force, pitch moment, yaw moment, and roll moment.

A 10 lb, strain gauge balance was used in the AFIT low-speed wind tunnel to record the force and moment measurements on all model configurations. The balance was manufactured by Modern Machine and Tool Company, Inc. Maximum allowable forces and moments were 10 lb normal force, 5 lb axial force, 5 lb side force, 10 in. · lb pitch moment, 4 in. · lb roll moment, and 5 in. · lb yaw moment [14].

Data reduction used the ambient conditions at the time of testing (e.g., room temperature and barometric pressure) and included several corrections. First, a correction for the solid blockage of flow in the wind tunnel caused by the model was made. Second, a downwash correction was made to correct for the effects of image vortices. Lastly, a conversion from the body axis to the wind axis was made through an Euler angle sequence. Additional details are provided in [13].

All tests for balance data were run at 30, 60, and 90 mph for Re variation and results consistency. These speeds were equivalent to approximately $Re = 0.1 \times 10^6$, 0.2×10^6, and 0.3×10^6, respectively. All AOA sweeps were from −4 to 22 deg. Flow visualization with the tufts was only accomplished at 10 and 15 deg AOA at 90 mph.

C. Flight-Test Configuration

The flight-test aircraft (tail number 68-8205) was an instrumented T-38A at the USAF TPS. Two accelerometers, corrected for their position with respect to the center of gravity of the aircraft, and an AOA sensor were used to determine the AOA and bank as a function of time. A 3 Hz moving average filter was applied to refine the data from the AOA sensor, the normal accelerometer, and the longitudinal accelerometer. Stick deflection was also captured as a function of time. Further information about the T-38 aircraft and systems can be found in the flight manual [5]. The replacement of the production nose boom with a flight-test nose boom and the addition of sensitive instruments used to gather performance data were assumed to have negligible effects on the aerodynamic and thrust characteristics of the aircraft. Therefore, the performance and stall characteristics of the test aircraft, without the wing fence, were considered production representative.

The test article was a wing fence that was attached to the T-38 at a 0.825 semispan on each wing. The preexisting attachment line at this wing station was used to attach the fence to the top and bottom surfaces of the wing. The aircraft wing span was not increased by the addition of the fences. The wing fence extended from the leading edge to 84.6% of the local chord length on the upper wing surface.

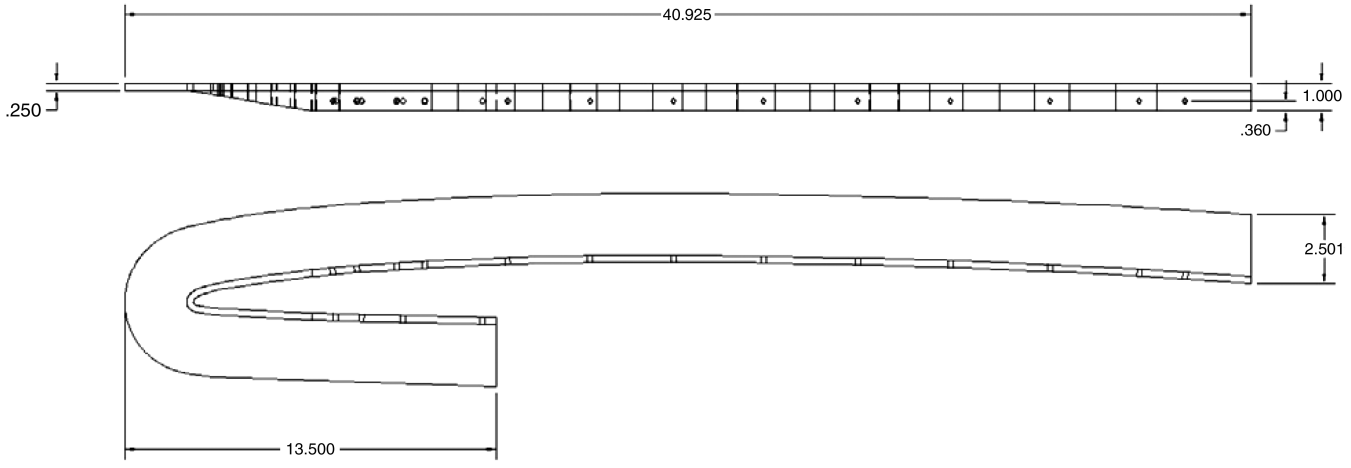

Fig. 4 Top and side views of flight-test wing fence (in inches).

The wing fence wrapped the leading edge and extended from the leading edge to 24.2% of the local chord length on the lower wing surface. This extension on the lower surface, over the wind-tunnel model, was required for fence attachment purposes. It had a constant height of 2.5 in. above the wing surface. Figure 4 shows a drawing of the fence. Each wing fence was made from two pieces of 6061-T6 aluminum. Both pieces were 0.25 in. thick and welded together. The wing fence was attached to the wing using 18 of the existing wing-tip fastener locations.

The Instrumentation Division of the USAF 412th Test Wing was responsible for the design implementation and structural analysis for the flight test. Structurally, the critical case was considered to be side loading from either the spanwise flow of air over the wing or with the aircraft in a side slip. An extremely conservative, maximum load of 7.65 psi was used, and an analysis for the fence and fasteners was accomplished to include stress and displacement. Lastly, an analysis on the weld was accomplished. All analyses showed the design to be adequate, and the fence was fabricated and installed. Figure 5 shows the installed wing fence on the left wing.

Data were collected on 10 sorties, including baseline and modified aircraft. Level decelerations, sawtooth climbs and descents, and approaches to stall were the flight-test techniques of choice. Level decelerations were executed with the aircraft initially at Mach 0.65, and the high-AOA data correspond to much lower values. Additional descriptions of the techniques are given in [13].

To collect flight-test flow visualization, the right wing was tufted for two sorties: one in the clean (baseline) configuration and one in the fence (modified) configuration. Tuft rows were in the streamwise direction and tuft columns were in the spanwise direction. There were four rows of tufts that extended from the wing tip to approximately 53 in. inboard of the wing tip. The four rows were located at 11.1, 33.4, 55.7, and 78.0% of the local chord. The tufts were separated by a minimum of two times the tuft length, approximately 6 in., to prevent entanglement. Figure 6 shows front- and side-view photographs of the installed tufts.

III. Results

A. Computational Fluid Dynamics

Figure 7a contains plots of C_L vs AOA for the clean configuration from 2 to 15 deg and for the fence configuration from 5 to 15 deg. As a reminder, this model had flaps in the full down position. The principal effect of the fence is a shift in the peak of the lift curve from 12 to 13 deg, with a corresponding 7% increase in $C_{L\,\max}$. Between 8 and 12 deg AOA, the fence configuration generates slightly higher lift than the clean wing. Below 8 deg AOA, the fence has no significant effect on lift production, which is consistent with prior studies. Interestingly, above 13 deg AOA, the fence again has little effect.

To determine where the increase in lift at 13 deg AOA occurs, the z component of the surface pressure force was sampled along several chord lines, from just outboard of the inlet to the tip, and integrated to generate sectional normal force plots for both wing configurations. The results, plotted in Fig. 7b, show that the fence configuration produces higher lift both outboard of the fence, which is consistent with past experimental data, and at the wing root, indicating that flowfield changes are not limited to the vicinity of the fence. The fence solution shows significantly greater suction along the leading edge, both outboard of the fence and near the wing root. This is an indicator that flow separation is reduced or eliminated over much of the wing.

An examination of in-plane velocity components in a constant-x plane located just aft of the wing-tip leading edge indicates the presence of a pair of vortices with opposite rotations: one adjacent to and outboard of the fence and another centered between the fence and the wing tip (Fig. 8). To better visualize these vortices, an isosurface of total pressure was generated to highlight the vortex structure, shown in Fig. 8. The isosurface shows well-defined fence and leading-edge vortices similar to those observed when a fence was placed at the break in a cranked wing [15]. The leading-edge vortex begins at the fence and is swept toward the trailing edge until it appears to merge with the wing-tip vortex. The fence vortex can be seen to lift from the surface, lose structure, and jump to the inboard side just forward of the end of the fence. The low pressure generated below this pair of vortices generates the suction responsible for keeping the flow outboard of the fence attached.

As discussed previously, a common explanation for the effects of a fence on thin swept wings (similar to the T-38) is that the fence acted as a barrier, preventing the growth of a leading-edge separation vortex originating at the wing root. To investigate this claim, a series of surface flow visualizations, shown in Fig. 9, were generated for the clean and fence configurations at AOAs of 5, 10, and 13 deg.

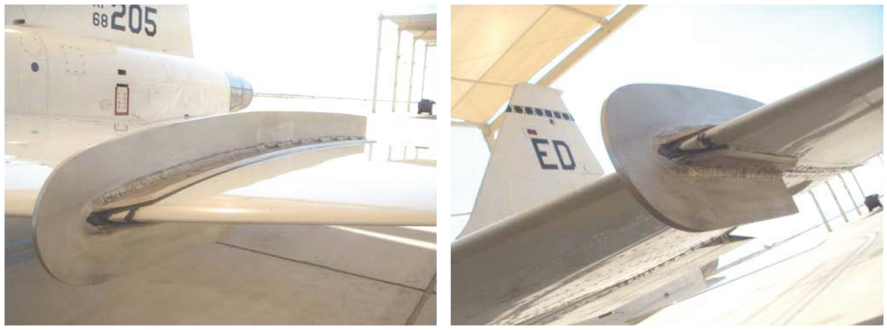

Fig. 5 Flight-test wing fence as installed on aircraft.

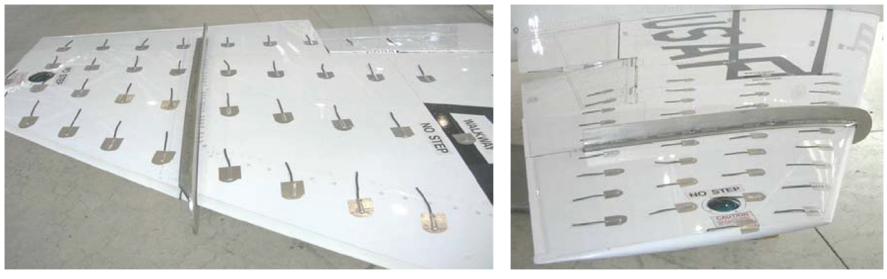

Fig. 6 Flight-test tufts, as placed on aircraft (front view and side view).

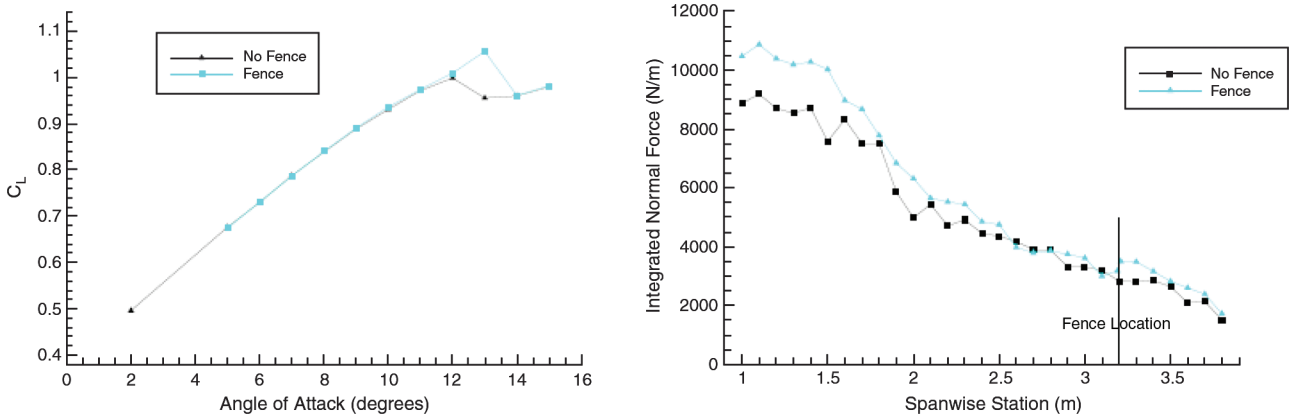

Fig. 7 Comparison of computed C_L, with and without wing fence (left), and comparison of computed sectional lift, with and without wing fence (right).

At 5 deg AOA, the clean-wing solution shows clear signs of a leading-edge vortex extending from the root and nearly to the wing tip. The addition of the fence clearly interrupts this vortex, but it appears to reform on the outboard leading edge. Surface flow over the majority of the wing remains unchanged.

At 10 deg AOA, the leading-edge vortex has been swept back to the trailing edge at approximately mid-semispan, and the trailing edge of the outer half of the wing is fully separated. Addition of the fence results in only small changes to flow on the inboard side. Flow outboard of the fence is significantly changed, with clear indications of the formation of both the fence and the strengthened leading-edge vortices. Most significantly, flow along the outer trailing edge remains attached.

At 13 deg AOA, significant differences in surface flow can be observed both inboard and outboard of the fence. On the clean wing, the trailing edge is completely separated, with all of the surface flow moving toward the leading edge. With the addition of the fence, the trailing edge remains attached. Inboard of the fence, flow along the leading edge is predominantly spanwise, with a weak separation line parallel to the leading edge terminating at the fence. Based on these computed results, it appears that the T-38 wing stall initially develops as a leading-edge separation vortex that develops at relatively low AOA. As the AOA increases, this vortex is swept aft, leading to separation at the tip trailing edge. As the AOA is further increased, the trailing edge separation moves inboard until the entire wing is stalled. The primary mechanism leading to improved lift with a fence above 8 deg AOA is the formation of the fence vortex and strengthening of the outboard leading-edge vortex, which together prevent the outboard trailing edge from separating. This leads to a delayed stall inboard of the fence. It does not appear that impeding growth of the initial leading-edge vortex plays a significant role in this case.

The changes in the surface flowfield that accompany the loss of effectiveness of the wing fence at 14 deg AOA can be seen in Fig. 9g. At this AOA, the wing inboard of the fence has stalled and closely resembles the clean-wing solution [16].

B. Wind Tunnel

The clean model was run three times at each velocity, with the wings taken on and off between runs to evaluate repeatability. Additionally, different conditions were varied by running the tunnel on different days. The resulting data were also used to derive the worst-case error bars, shown in Fig. 10. Also seen in Fig. 10 are some basic Reynolds number effects. Repeatability and error analysis were considered acceptable.

The lift coefficients were also compared between the clean and fence configurations at 13.6 deg AOA. The reported errors are based on the worst-case errors at each velocity. At 30 mph, the clean C_L was 0.588 ± 0.005, and the fence C_L was 0.634 ± 0.005. At 60 mph, the clean C_L was 0.640 ± 0.004, and the fence C_L was 0.665 ± 0.004. At 90 mph, the clean C_L was 0.655 ± 0.003, and the fence C_L was 0.683 ± 0.003.

Figure 11 provides evidence of mild increase in the maximum lift coefficient when the wing fence is in place. The wind-tunnel data for the clean configuration and the wing-fence models were acquired for the 90 mph (40 m/s) case. The average maximum increase in C_L for the 90 mph case to the clean configuration was 0.039, which equated to an increase of approximately $4.3 \pm 0.6\%$. The computed results for the wing with flaps deployed but without the wing fence are also given in this figure to demonstrate that the break in the lift curve generally corresponds with the data. In addition to differences in the geometry, the Reynolds number for the CFD model was an order of magnitude larger, which likely influenced the severity of the break in the lift curve.

The flow visualization observations were made at 10 and 15 deg AOA, at approximately $Re_{\text{mac}} = 0.3 \times 10^6$. This section compares clean and fence configurations at both AOAs with a side view presented first, followed by a top view, as seen in Figs. 12a–12h.

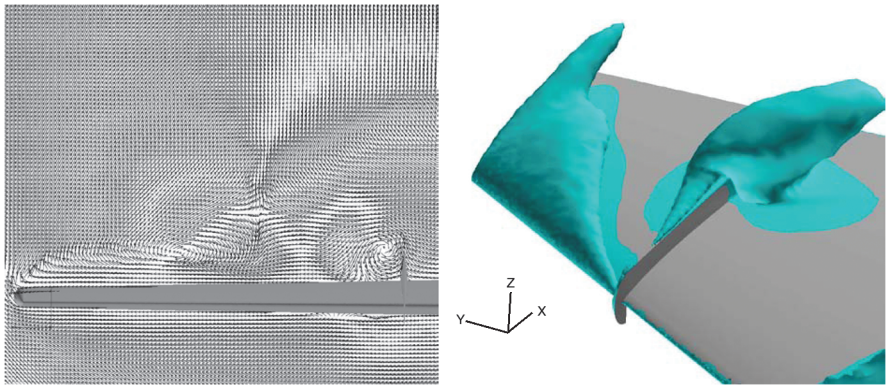

Fig. 8 Normalized in-plane velocity vectors for constant X plane, located just aft of the leading edge at the wing tip (left) and isosurface of total pressure (9.89E4 Pa), showing locations of fence and leading-edge vortices (right).

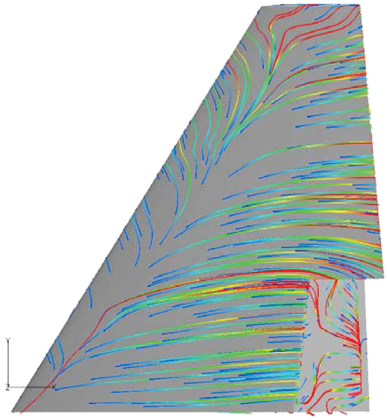

a) 5° AOA, no fence

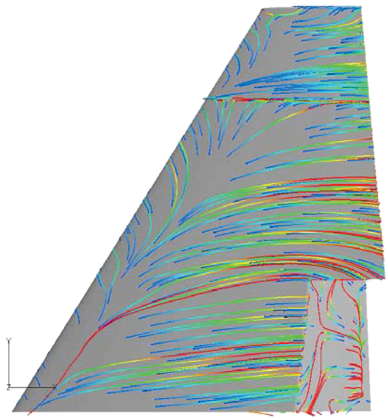

b) 5° AOA, fence

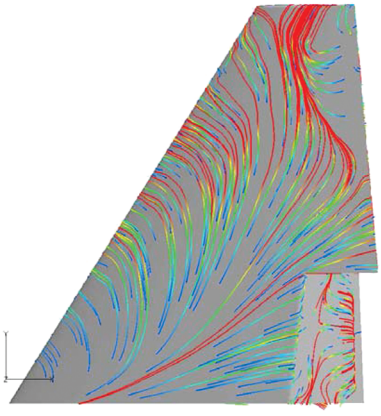

c) 10° AOA, no fence

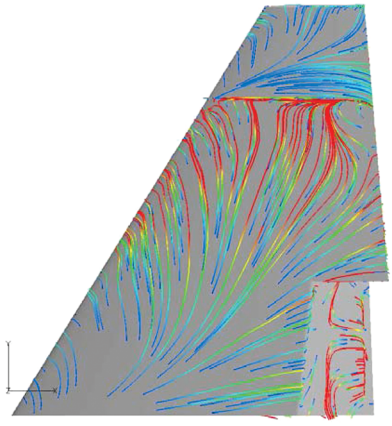

d) 10° AOA, fence

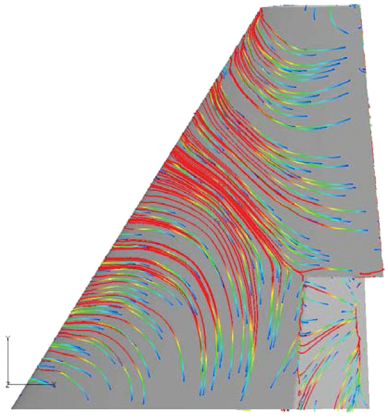

e) 13° AOA, no fence

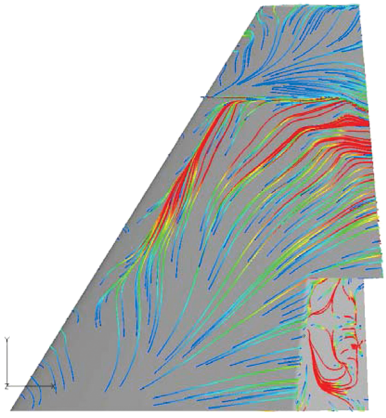

f) 13° AOA, fence

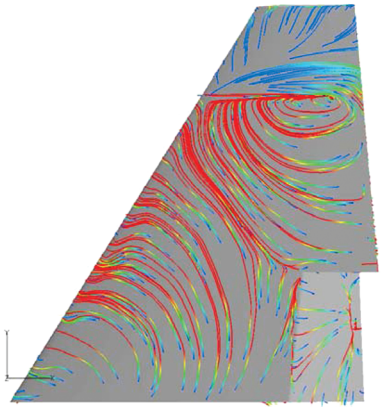

g) 14° AOA, fence

Fig. 9 CFD upper surface flow with and without wing fence, with flow direction indicated by a blue to red gradient.

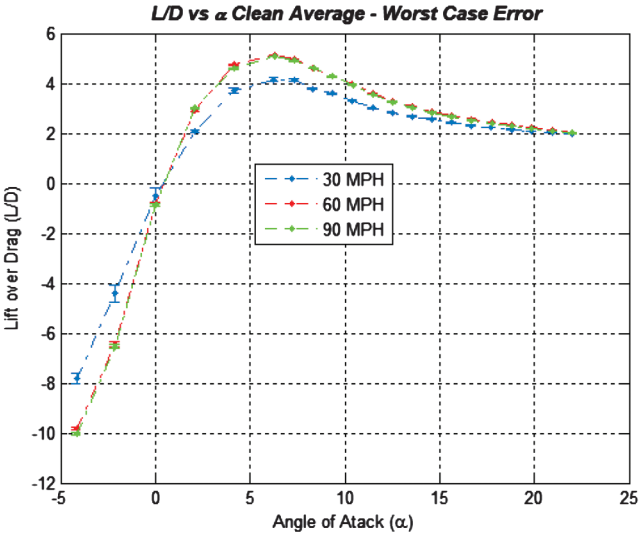

Fig. 10 Wind-tunnel clean lift to drag with worst-case error bars.

At 10 deg AOA and in the side view, the clean wing showed some significantly reversed flow in the second row on the outer two-thirds of the wing. The inboard one-third was attached in the second row. In the first row, there were areas of thick boundary layer as well as a few areas of reversed flow. In the case of the fence, the first row was very similar, except that the flow just outside the fence was attached. Also, in the second row, the second through the tenth tufts in from the wing tip showed much more streamlined attached flow. The fence significantly altered the flow over the wing in its vicinity. There was some effect inboard of the fence where the spanwise flow was directed in the streamwise direction. However, most of its impact was outboard of the fence.

The top view shed further light on the side view. In the first row on the clean wing, significant spanwise flow existed for almost the entire semispan. In the second row, the middle-third showed spanwise flow toward the tip that transitioned into reversed flow and then to flow moving toward the fuselage. The spanwise flow was almost completely removed by the fence, except for the second tuft in from the wing tip on the first row. The fence clearly had some impact on the flow inboard of the fence and a significant impact on the flow outboard of the fence, particularly in arresting spanwise flow and increasing the amount of attached flow on the wing.

At 15 deg AOA, the clean wing was almost entirely stalled. In the side view, the clean wing showed significantly reversed flow in the entire second row. The first row was essentially the same but not as heavily reversed. In the case of the fence, the first and second rows were very similar to the clean wing, except that just inboard and completely outboard of the fence was no longer detached. The fence had significantly altered the flow over the wing in its vicinity for the better.

Again, the top views shed further light on the results seen in the side-view photographs. In the first row for the clean wing, significant spanwise flow existed for the entire semispan. In the second row for the fence, the spanwise flow of the outer five tufts in both rows was almost completely removed. The fence clearly had a significant impact on the flow both inboard and outboard of the fence, particularly in arresting spanwise flow as well as increasing the overall amount of attached flow on the wing.

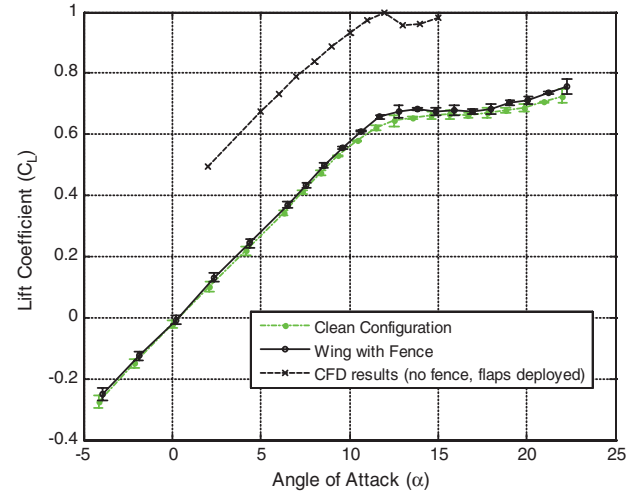

Fig. 11 Lift curves from the wind-tunnel runs acquired at 90 mph (40 m/s) for the clean configuration and the model with the wing fence. The CFD results (see Fig. 7) are also given for the flaps-deployed case (no wing fence) for comparison.

C. Flight Test

Ten flight-test sorties, totaling 11.4 h, were accomplished from 19 September 2008 to 10 October 2008 at Edwards AFB, California, as described in [13]. Lift coefficients of the baseline and modified aircraft were compared through the collection of data via level decelerations with and without the fence. Ten total maneuvers were used here, with four without the fence and five with the fence. The computed results yielded data scatter of approximately 2 deg AOA at $C_L = 0.72$. Therefore, further analysis was necessary. The data from 12–14.5 deg AOA were subsampled down to 5 Hz. Regression and analysis of variance analyses were accomplished, yielding a 1.8–3.8% increase in C_L at about 13.5 deg AOA. An additional way (most viewable for data presentation) the subsampled data set was analyzed is shown in Fig. 13. All of the data in each 0.5 deg group (12–12.5, 12.5–13, 13–13.5, 13.4–14, and 14–14.5 deg) were averaged to create one data point of AOA and C_L for that group. This was accomplished for both the fence and no-fence conditions. The error bars are 95% confidence intervals for each separate data set. The average C_L was increased by the fence over the clean configuration in each group. However, because the confidence intervals overlap in all cases, except 14–14.5 deg, this increase cannot be reported with 95% confidence.

An important point when considering these results as compared with the wind-tunnel results is the absence of the wind-tunnel model tail. The reference area for the T-38 tail is 59 and 170 ft^2 for the wing. A simple area analysis, ignoring fuselage contribution, shows that the wind-tunnel results (fence impact on C_L) could be as much as 25% greater than flight-test results. Assuming that the fence impact on lift coefficient was the same in the wind tunnel and the flight test, its contribution would be a lower percentage of the overall lift coefficient.

The approach-to-stall characteristics were investigated qualitatively through pilot observations and comments and quantitatively through simple measurements of AOA, lateral stick position, and bank angle. The approach-to-stall characteristics of each configuration were evaluated in the following way: the pilot attempted to maintain the control stick centered laterally (stick-fixed) while stabilizing at successively higher AOA. and the pilot comments about controllability, buffet onset and intensity, uncommanded rolls, and stick deflection were noted. The aircraft data acquisition system recorded AOA, lateral stick deflection, and bank angle.

In both the baseline (clean) and the wing-fence modified aircraft, the approach to stall was characterized by moderate buffet, wing rock (characterized by observed high-frequency oscillation), and low-frequency bank-angle oscillations. An example of the flight-test data for a baseline case is given in Fig. 14, whereas data for the aircraft with the wing-fence modification is given in Fig. 15. Each set of flight test data shown corresponds to a stick-fixed scenario.

The stick-fixed clean configuration showed bank-angle oscillations of up to ± 11 deg with a period of approximately 25 s. Wing rock overlaid the bank-angle oscillations and was characterized by quick, shallow, alternating wing dips with a period of approximately 2 s. The wing-rock magnitude was as much as ± 9 deg. The aircraft started the approach to stall with wings level but then rolled left to about 20 deg of bank, where the bank-angle oscillations and wing

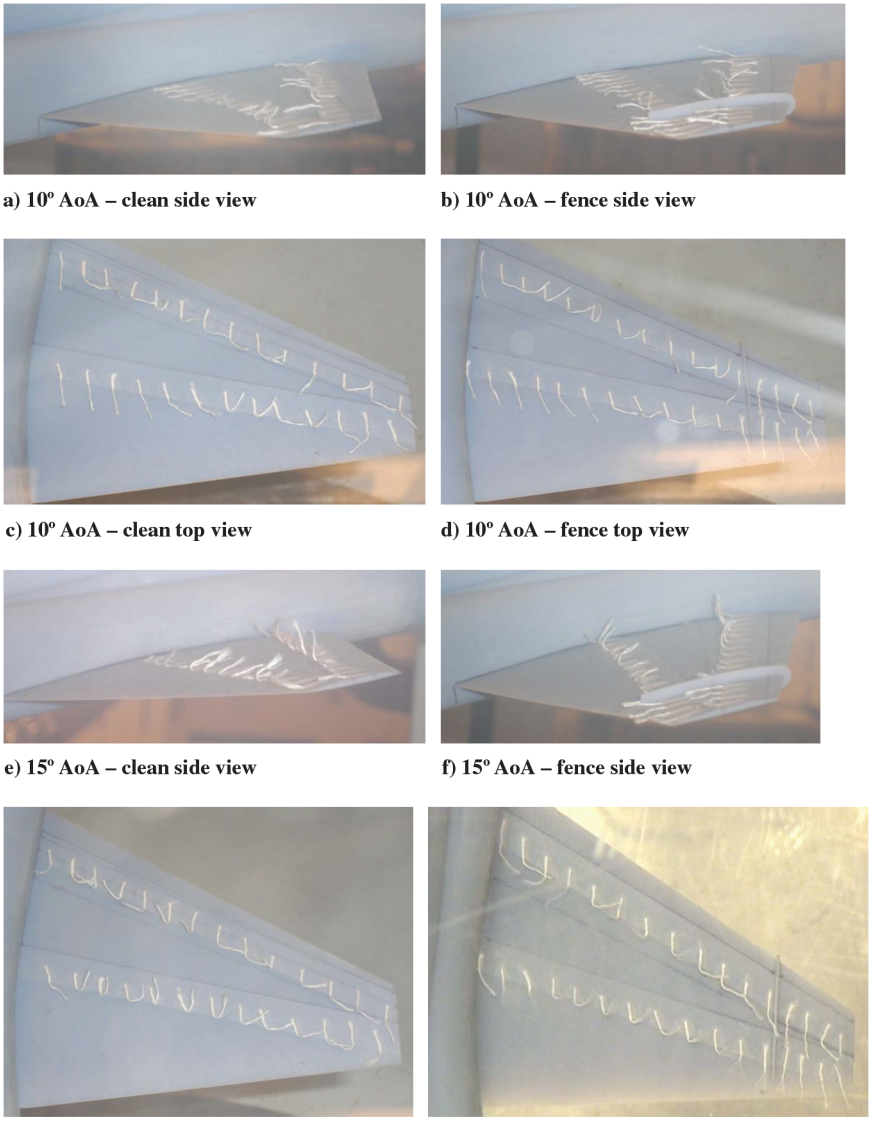

a) 10° AoA – clean side view

b) 10° AoA – fence side view

c) 10° AoA – clean top view

d) 10° AoA – fence top view

e) 15° AoA – clean side view

f) 15° AoA – fence side view

g) 15° AoA – clean top view

h) 15° AoA – fence top view

Fig. 12 Wind-tunnel flow visualization, with and without wing fence.

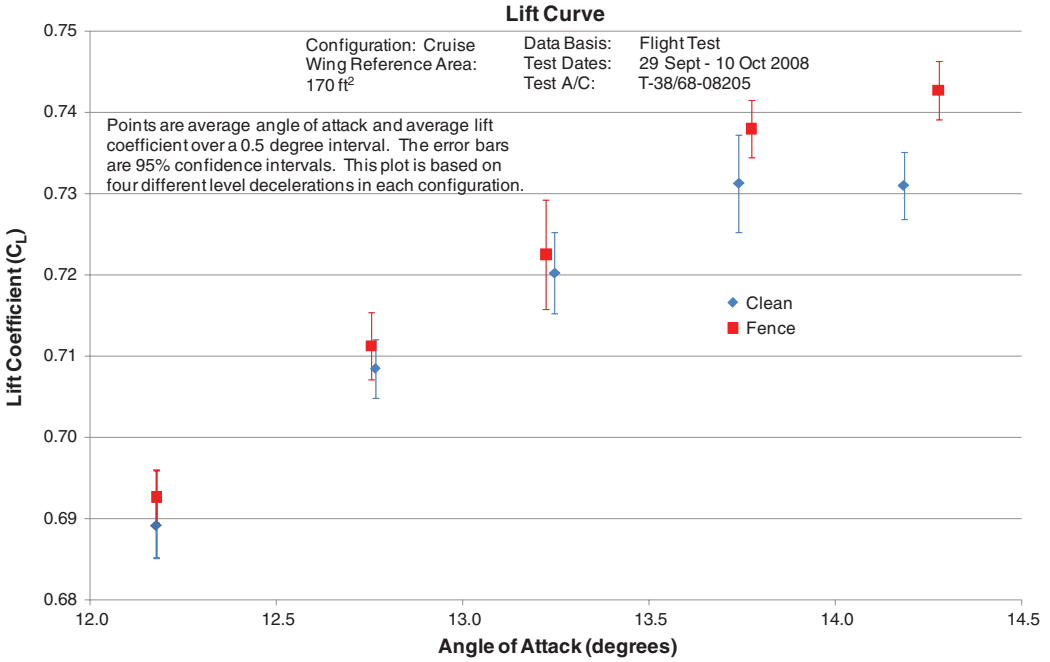

Fig. 13 Flight-test lift curve: clean vs fence.

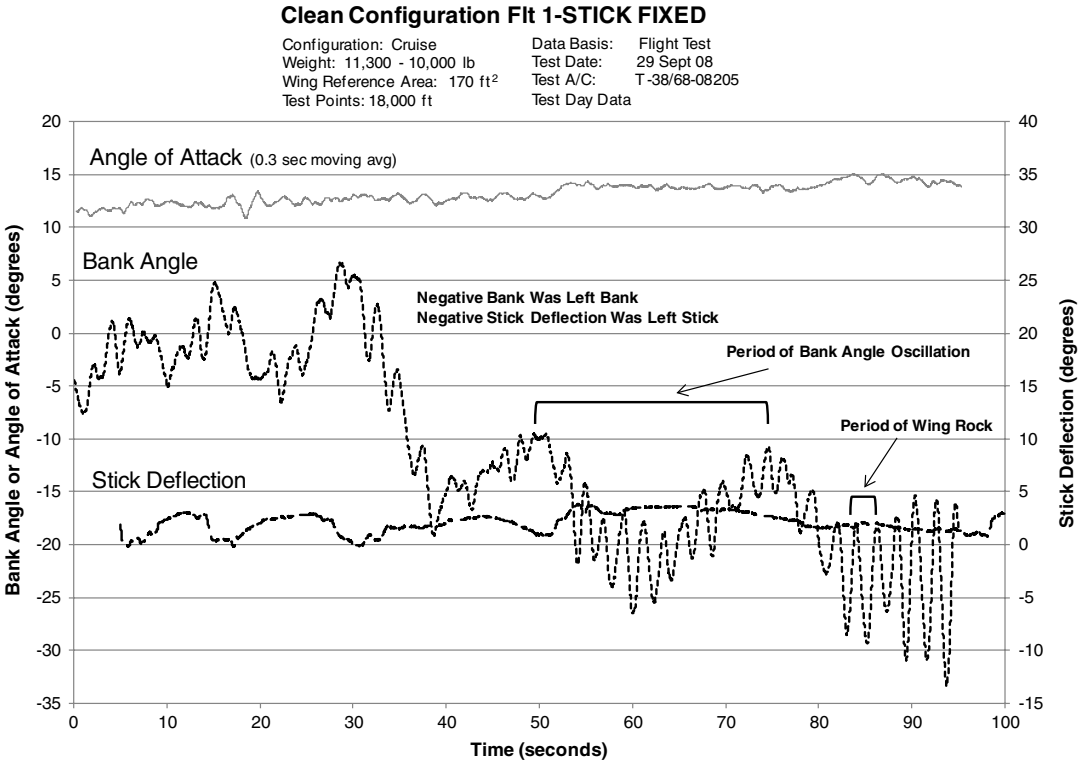

Fig. 14 Flight-test clean approach-to-stall data.

rock were then centered around. This occurred even though there was 3 deg of right stick deflection during the left roll off.

The stick-fixed modified configuration showed bank-angle oscillations of up to ±8 deg with a period of 20 s, as can be seen in Fig. 15. Wing rock had a period of approximately 2 s and a magnitude of up to ±4 deg. The aircraft started the approach to stall with wings level and rolled left to only about 5 deg of bank, around which wing-rock and bank-angle oscillations were centered. This occurred with about 0.5 deg of left stick deflection.

The wing fence improved the approach-to-stall characteristics. The bank-angle oscillations were decreased from 22 to 16 deg. Wing-rock oscillations were decreased from 18 to 8 deg. Considering that the wing-rock periods were about the same, the difference in amplitudes made a significant difference in the roll rates experienced

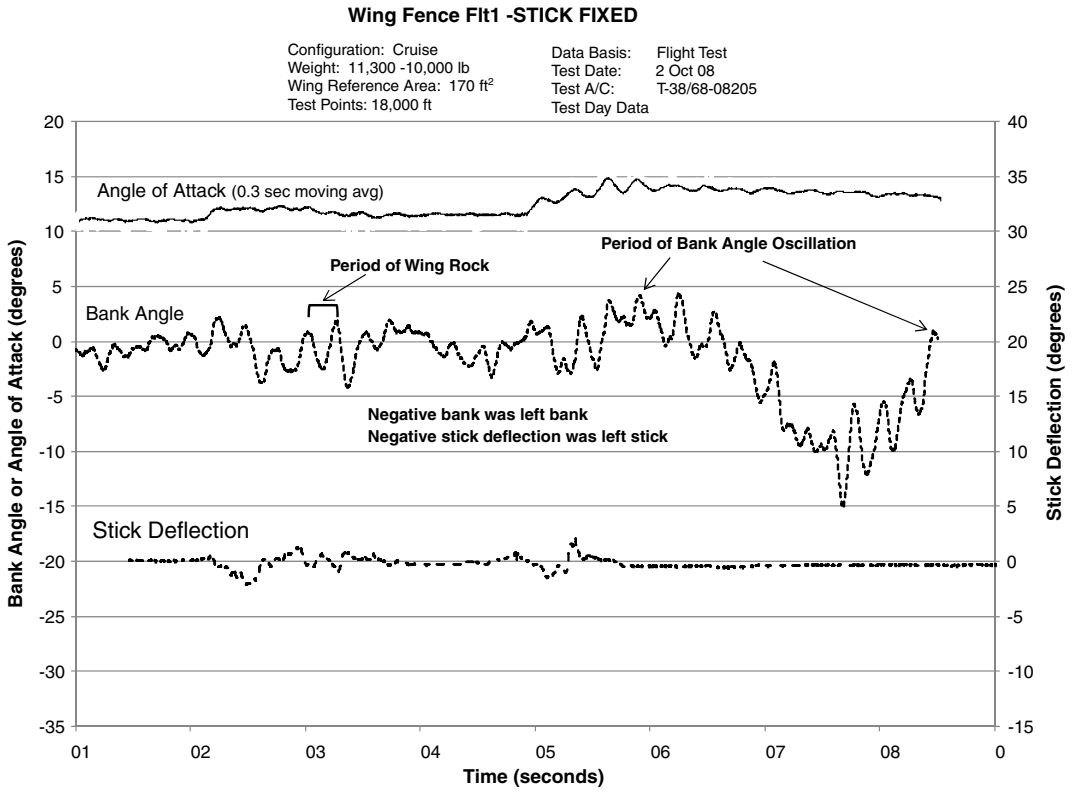

Fig. 15 Flight-test fence approach-to-stall data.

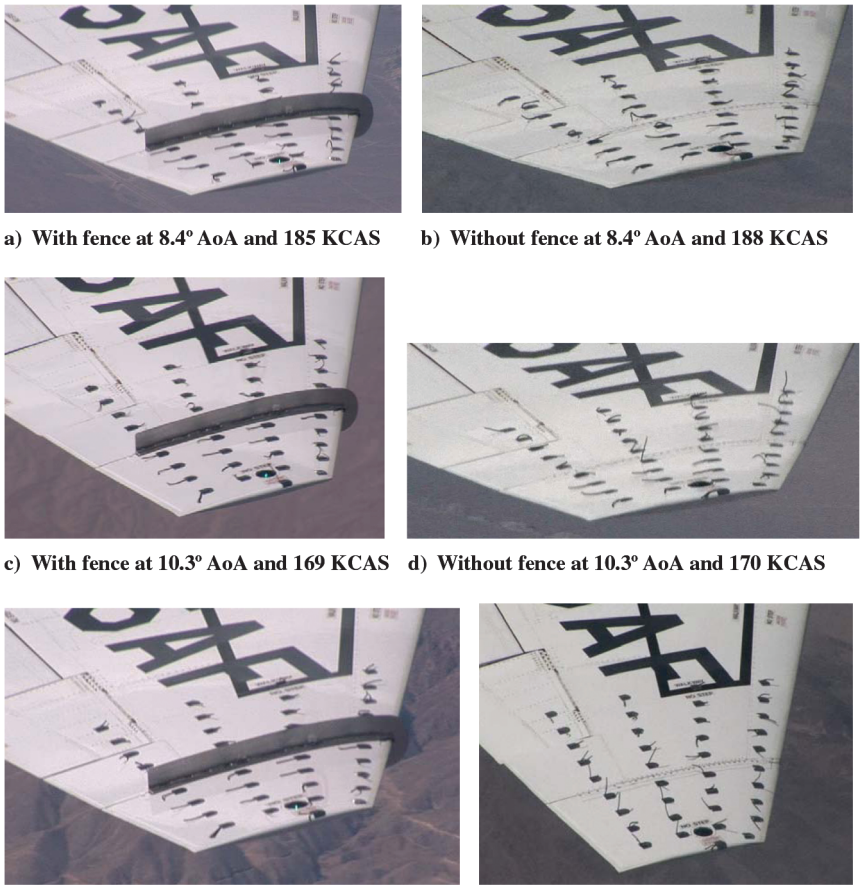

a) With fence at 8.4° AoA and 185 KCAS b) Without fence at 8.4° AoA and 188 KCAS

c) With fence at 10.3° AoA and 169 KCAS d) Without fence at 10.3° AoA and 170 KCAS

e) With fence at 14.9° AoA and 153 KCAS f) Without fence at 14.9° AoA and 152 KCAS

Fig. 16 Flight-test flow visualization of the upper surface of the T-38 starboard wing, with and without wing fence.

by the pilot during the approach to stall. This was qualitatively observed and noted in a daily flight report. Additionally, a pilot comment was that addition of the wing fence slightly reduced buffet intensity. According to the pilot, the buffet for both configurations was moderate, but the random aperiodic spikes, characteristic of a T-38, were not as severe with the wing fence installed. Lastly, the wing-fence modified aircraft did not lead to the large left roll off experienced by the clean aircraft.

Flight-test flow visualization is shown in Figs. 16a–16f. At 8.4 and 10.3 deg AOA, the flow outboard of the wing-fence/seam (location on the clean wing where the fence was installed) was similar for both configurations. Though not shown, this was true through 12.4 deg AOA. Specifically, the outer three columns of tufts were nearly identical between configurations. The exception was the column of tufts immediately outboard of the fence/seam. On the clean wing, this column of tufts showed separated and reversed flow for nearly the full chord length. However, with the fence installed, the same column of tufts was streamlined and indicated attached flow.

At 14.9 deg, the flow outboard of the seam on the clean wing was completely separated. The tufts were all standing straight up or reversed, as evident in Figs. 16e and 16f. The impact of the fence was even more apparent at this AOA. Contrary to the clean wing, the flow over the wing area outboard of the fence was primarily attached and in the streamwise direction.

IV. Conclusions

A comprehensive study was undertaken with the goal of improving the flight safety of the T-38. Specifically, the goal was to determine whether a straightforward modification of the aircraft wing with a fence would improve the aircraft's high-AOA performance and approach-to-stall characteristics. The nature of the retrofit mandated that the fence be placed farther from the fuselage than most other fences used on other aircraft, especially given the large taper ratio for the T-38 wing. At issue was whether a fence at an outboard location would have the desired effect. The study included CFD studies, wind-tunnel testing, and full-scale flight testing. Each set of tests suggested that the lift curve and overall approach-to-stall characteristics were enhanced at high AOA when the fence was installed and, furthermore, suggested that the reason for the improvement is that flow remained attached over a portion of the wing.

Computational results suggested that a fence that wrapped around the leading edge and extended far above the boundary layer increased $C_{L\max}$ by 7% and delayed the achievement of $C_{L\max}$ from 12 to 13 deg AOA. This effect was achieved through the formation of a discrete vortex outboard of the fence that prevented flow separation in that region. Preventing separation at the outer trailing edge effectively delayed flow separation of the remainder of the wing, resulting in the higher computed lift.

Wind-tunnel studies were performed on a variety of fence designs, and it was found that the addition of a wing fence of the geometry used in the CFD study, placed at a 0.825 semispan, increased C_L by $4.3 \pm 0.6\%$ for the highest fidelity test case. Flow visualization with tufts confirmed the behaviors predicted in the CFD study. The wing fence increased the area of the region of streamlined flow on the surface of the wing, primarily outboard of the fence. Given that the data suggested the fence used in the CFD study was the optimal geometry of those investigated, it was decided to flight test that design.

Flight tests additionally indicated an average increase in C_L with the fence, though it should be noted that the error bars overlapped the average of the clean configuration at the 95% confidence interval. Accelerometer data and pilot comments suggested that the wing fence improved the approach-to-stall characteristics. The wing-fence modification reduced the roll-off tendency above 9 deg AOA during the approach to stall and reduced the wing-rock magnitude from 18 to 8 deg of bank angle. Additionally, with the fence, the aircraft was essentially less sluggish in roll, allowing the pilot to keep the

aircraft's wings level more easily. Tufts applied to the wing surface also provided insight into the flow dynamics. Whereas only small differences in flow characteristics were noted at AOAs below 12.4 deg, observed flow characteristics indicated that the wing fence significantly decreased separated flow at AOAs above 13.9 deg.

The results of this study suggest that a wing fence placed at the preexisting seam in the wing of the T-38 (at the 0.825 semispan) does mildly improve the high-AOA performance. Whether that improvement is significant and whether it might lead to undesirable consequences remains an open question. For example, the behavior of the fence in the presence of yaw and its impact on aerodynamic efficiency at typical cruise conditions were not considered in this study. In addition, the computational results and wind-tunnel tests indicate that a wing fence may create a more pronounced break in the lift–curve slope, which could offset the flight safety benefits of improved stall characteristics.

Acknowledgments

The authors would like to acknowledge the support of Hugh Thornburg of the U.S. Air Force Research Laboratory, Major Shared Resource Center, who was extremely helpful with the computational fluid dynamics and wind-tunnel model drawings. The authors would also like to thank Jay Anderson and John Hixenbaugh for their assistance in preparing the wind-tunnel models and assisting in the tests. The authors would like to acknowledge the assistance of Jonathan Dietrich, Joshua Schneider, Matthew Wroten, and Gian Luca Greco as the flight-test team members, playing integral roles in meeting the flight-test objectives. The views expressed in this paper are those of the authors and do not reflect the official policy or position of the U.S. Air Force, the Department of Defense, or the U.S. Government.

References

[1] "Fact Sheet: T-38 Talon," U.S. Air Force, 2006, http://www.af.mil/information/factsheets/factsheet.asp?id=126 [accessed Aug. 2009].

[2] Nickel, K., and Wohlfahrt, M., *Tailless Aircraft*, 1st ed., AIAA, New York, 1994.

[3] Zhidkosti, M., "Flow on a Swept Wing in the Region of a Fence," *Fluid Dynamics*, Vol. 3, No. 6, July 1968, pp. 84–86. doi:10.1007/BF01022888

[4] Rossow, V., "Two-Fence Concept for Efficient Trapping of Vortices on Airfoils," *Journal of Aircraft*, Vol. 29, No. 5, Sept.–Oct. 1992, pp. 847–855. doi:10.2514/3.46255

[5] "T-38 A/B Flight Manual," published under the authority of the Secretary of the U.S. Air Force, 01 July 1978.

[6] Queijo, M. J., Jaquet, B., and Wolhart, W., "Wind Tunnel Investigation at Low Speed of the Effects of Chordwise Wing Fences and Horizontal Tail Position on the Static Longitudinal Stability Characteristics of an Airplane Model with a 35 deg Sweptback Wing," NACA, Rept. 1203, 1954.

[7] Strang, W., Tomaro, R., and Grismer, M., "The Defining Methods of Cobalt-60: A Parallel, Implicit, Unstructured Euler/Navier–Stokes Solver," 37th Aerospace Sciences Meeting and Exhibit, AIAA Paper 99-0786, Jan. 1999.

[8] "SolidMesh 3D User's Manual," [online user's manual], http://www.simcenter.msstate.edu/docs/solidmesh/, Mississippi State Univ., Mississippi, MS, [retrieved 28 Dec. 2007].

[9] Marcum, D. L., "Efficient Generation of High Quality Unstructured Surface and Volume Grids," *Engineering with Computers*, Vol. 17, No. 3, 2001, pp. 211–233. doi:10.1007/PL00013386

[10] Solfelt, D. A., "CFD Analysis of a T-38 Wing Fence," Master's Thesis, Air Force Inst. of Technology, Dept. of Aeronautics and Astronautics, Wright–Patterson Air Force Base, OH, June 2007.

[11] Vavilis, P. S., and Ekaterinaris, J. A., "Computational Investigation of Flow Control over Wings," Aerospace Sciences Meeting and Exhibit, AIAA Paper 2007-477, Jan. 2007.

[12] Forsythe, J. R., Squires, K. D., Wurtzler, K., and Spalart, P. R., "Detached-Eddy Simulation of the F-15E at High Alpha," *Journal of Aircraft*, Vol. 41, No. 2, March 2004, pp. 193–200. doi:10.2514/1.2111

[13] Williams, M. D., "Wind Tunnel Analysis and Flight Test of a Wing Fence on a T-38," Master's Thesis, Dept. of Aeronautics and Astronautics, Air Force Inst. of Technology, Wright–Patterson AFB, OH, March 2009.

[14] "*AFIT-1 Balance Operator Manual*," Modern Machine and Tool, Newport News, VA, 2004, pp. 16–18.

[15] Rao, D. M., "Subsonic Flow Investigations on a Cranked Wing Designed for High Maneuverability," NASA, Cont. Rpt. 178046, 1986.

[16] Solfelt, D. A., and Maple, R. C., "CFD Analysis of a T-38 Wing Fence," 46th AIAA Aerospace Sciences Meeting and Exhibit, AIAA Paper 2008-331, Jan. 2008.